Single photon simultaneous K-shell ionization/excitation in C 6 H 6 : experiment and theory

S. Carniato, P. Selles, A. Ferté, N Berrah, A H Wuosmaa, M Nakano, Y. Hikosaka, K. Ito, M. Žitnik, K. Bučar, et al.

Single photon simultaneous K-shell ionization/excitation in C_6H_6: experiment and theory.

S. Carniato [1], P. Selles[1], A. Ferté[1], N. Berrah[2], A. H. Wuosmaa[2], M. Nakano[3], Y. Hikosaka[4], K. Ito[3,5], M.Žitnik[6], K. Bučar[6], K. Soejima[7], K. Jänkälä[8], D. Cubaynes[5,9], J.-M. Bizau[5,9], L. Andric[1], M. Khalal[1], J. Palaudoux[1], P. Lablanquie[1] and F. Penent[1,*]

[1] Laboratoire de Chimie Physique-Matière et Rayonnement (UMR 7614), Sorbonne Université, CNRS, 4 Place Jussieu,75252 Paris Cedex 05, France

[2] Department of Physics, University of Connecticut, Storrs, Connecticut 06269, USA

[3] Photon Factory, Institute of Materials Structure Science, Tsukuba 305-0801, Japan

[4] Institute of Liberal Arts and Sciences, University of Toyama, Toyama 930-0194, Japan

[5] Synchrotron SOLEIL, L'Orme des Merisiers, Saint-Aubin, Boîte Postale 48, 91192 Gif-sur-Yvette Cedex, France

[6] Jožef Stefan Institute, Jamova Cesta 39, SI-1001 Ljubljana, Slovenija

[7] Department of Environmental Science, Niigata University, Niigata 950-2181, Japan

[8] Nano and Molecular Systems Research Unit, University of Oulu, P.O. Box 3000, 90014 Oulu, Finland

[9] ISMO, CNRS UMR 8214, Université Paris-Sud, Université Paris-Saclay, 91405 Orsay, France

[*] corresponding author: francis.penent@upmc.fr

Abstract. Single photon simultaneous core ionization/core excitation ($K^{-2}V$) of the Benzene molecule has been observed experimentally, using synchrotron radiation, by electron coincidence spectroscopy with a magnetic bottle time-of-flight electron spectrometer and reveals a rich spectrum. DFT and Post-Hartree-Fock calculations provide detailed assignments of $K^{-2}V$ states. The specific Auger decay of these states has also been determined experimentally with a new technique to improve the energy resolution.

PACS numbers: 33.20.Rm, 33.60.+q, 33.80.Eh

Keywords: Photoionization, electron spectroscopy, double core-hole, XPS, NEXAFS

1. Introduction

Thanks to the advent of XFEL sources allowing simultaneous absorption of two photons and, in parallel, to the improvements of electron coincidence spectroscopy technique on 3^{rd} generation synchrotron sources allowing the observation of double core ionization processes by a single photon, Double Core Hole (DCH) spectroscopy has become a growing research field for both experiment and theory [1, 2, 3, 4, 5, 6, 7, 8, 9, 10]. Seminal predictions by Cederbaum et al [11] anticipating the interest of this kind of spectroscopy for the determination of electronic-structure information not accessible by conventional spectroscopies [12] could then be validated.

In our recent paper [13] single-site Double-Core Hole (ss-DCH or K^{-2}) and two-site Double-Core Hole (ts-DCH or $K^{-1}K^{-1}$) spectroscopy of Benzene molecule were investigated both experimentally and theoretically. Some discrepancies with previous interpretations [14, 15] indicate that DCH spectroscopy must also rely on accurate theory taking into account subtle correlation and relaxation effects. The ejection of two core electrons induces a very strong perturbation on the outer orbitals and simultaneous excitation of a valence electron corresponding to the formation of $K^{-2}v^{-1}V$ satellite states is enhanced compared to the $K^{-1}v^{-1}V$ satellites observed in single K-shell ionization. Recent theoretical developments [16] have improved the interpretation of DCH spectra with accurate calculation of energy levels and of relative cross-sections, showing the interest of a field challenging for theory.

A complementary aspect of double K-shell ionization is the process consisting in K-shell ionization of one electron with simultaneous excitation of the other K-electron to a vacant orbital. This so-called $K^{-2}V$ process was studied on other systems [17, 18] and can be interpreted as a special case of K^{-1} satellite with super shake-up excitation of the second K-shell electron. This process could also be accompanied by simultaneous shake-up of a valence electron v giving rise to double shake-up states: $K^{-2}Vv^{-1}V$' but we will keep the $K^{-2}V$ general denomination throughout the text for sake of simplicity. In the mathematical expansion of the theoretical cross-section that describes this process, two kinds of terms appear that correspond to the transfer of the photon angular momentum either to the outgoing ionized electron (direct process) or to the excited electron (conjugate process).

Close to the single-core ionization threshold, shake-up can only involve a valence electron: $K^{-1}v^{-1}V$ and the intensity of co-existing direct or conjugate shake-up transitions [19] changes strongly with photon energy. Far above threshold, where sudden-approximation should be appropriate, these shake-up satellites are created essentially by direct processes, i.e., a core electron is dipole ionized and a valence electron is excited via a monopole transition.

Close to the double-core ionization threshold, however, conjugate shake-up processes, involving dipole excitation of a core electron to a vacant valence orbital and monopole ionization (shake-off) of the other core electron are also possible. In contrast with direct shake-up transitions, the final states of conjugate transitions may

have symmetries different from that of the core-ionized state giving rise to new peaks in the photoelectron spectrum since the photon angular momentum can be carried out either by the excited or by the ionized electron.

Since the binding energy of $K^{-2}V$ states is quite far (roughly a factor 2) from the single core ionization threshold, the conjugate path should be negligible. Nonetheless, experiments supported by a theoretical model [20] providing absolute photoionization cross-sections for $K^{-2}V$ ionization process, have shown that both direct and conjugate routes are, indeed, very weak ($\sim 10^{-4}$ vs K^{-1}) but present similar magnitudes. This could also be interpreted as aborted double core ionization (two correlated electrons absorbing a single photon) where one of the two outgoing electrons is finally recaptured by the doubly charged ion. The photon angular momentum can hence be carried out by any of the two electrons with similar probabilities.

With $K^{-2}V$ spectroscopy it becomes possible to probe, not only unoccupied levels revealed by NEXAFS (Near-Edge X-Ray Absorption Fine Structure) spectroscopy, but also dipole-forbidden [18] transitions (that can only appear in NEXAFS through vibronic coupling effect). It also provides a way to measure experimentally the magnitude of band shifts between $K^{-1}V$ vs $K^{-2}V$ states and, accordingly, to bring additional information to discuss the Valence or Rydberg character [21] of the core excited states lying close to the ionization thresholds. Finally, it shows to what extent our theoretical model [9, 20, 21] is accurate to reveal the nature (direct or conjugate) of $K^{-2}V$ states of Benzene and to provide an estimation of the cross-sections.

Since only one photo-electron is released in the $K^{-2}V$ process, X-ray Photoelectron Spectroscopy (XPS), using conventional hemispherical electron analyzer, can be performed [22, 23] as far as the corresponding photoelectron energies are well isolated from other dominant processes (single K-shell ionization). This has opened the way of $K^{-2}V$ spectroscopy on tender x-ray synchrotron beam lines ($\geq$2.3 keV).

Concurrently, electron coincidence spectroscopy with a magnetic bottle time-of-flight electron spectrometer [2, 21] can provide also high resolution $K^{-2}V$ spectroscopy on single molecular systems at photon energies close to the double K-shell ionization threshold (about 650 eV for Carbon K^{-2}, 900 eV for Nitrogen). Moreover, the coincidence technique allows also to extract the specific cascade Auger decay of these states.

These two experimental techniques can be used for $K^{-2}V$ spectroscopy that presents the characteristics of both XPS (emission) and NEXAFS (absorption) spectroscopies. They are also complementary: the magnetic bottle integrates the signal on the full solid angle and relies on absolute cross-sections while XPS is sensitive to the angular distribution of photoelectrons that depends on the angular momentum it carries out [18].

The benzene molecule, that is often used as a textbook example for any kind of spectroscopy, and was also chosen for ss-DCH (K^{-2}) and ts-DCH ($K^{-1}K^{-1}$) spectroscopy [13], is expected to be also a simple theoretical playground for $K^{-2}V$ spectroscopy with six equivalent carbon atoms. In the present paper, we present the complex $K^{-2}V$

spectra of C_6H_6, that was obtained experimentally and a precise theoretical approach. Furthermore, the Auger decay of these states has also been observed experimentally with a good resolution.

2. Experimental details

The present results were obtained at the undulator beamline SEXTANTS [24] of the synchrotron SOLEIL in St Aubin, France, with our magnetic bottle time-of-flight (MB-TOF) electron spectrometer (HERMES). Single-bunch operation of the storage ring in top-up mode provides stable light pulses with 1184 ns repetition period. All details of the experimental procedure were given in our previous publications [13, 20, 21] and there is no need to recall them here. The same raw data set that was used to extract K^{-2} and $K^{-1}K^{-1}$ processes in C_6H_6 [13] was also used to extract the present $K^{-2}V$ spectra. Afterwards, additional results were obtained with a modification of our experimental set-up allowing to decelerate the electrons in the TOF to improve the energy resolution. A 2m long insulated non-magnetic titanium tube (89 mm inner diameter), polarized at -V potential, is inserted in the CF100 vacuum tube on which the solenoid is wound. The deceleration of all the electrons is done between two parallel high transmission ($\sim 95\%$) gold grids separated by 3 mm, the first one is grounded and the second one at -V potential is at the entrance of the flight tube. Between the two grids, there are no lensing effects that could change the length of electron trajectories and the electrons remain on their initial magnetic field lines. The performance of the deceleration method on the energy resolution will be demonstrated in the paragraph showing the Auger spectra.

3. Theoretical building blocks

$K^{-2}V$ cross sections can be obtained on an absolute scale thanks to the theoretical model that we have developed and applied successfully previously [9, 20, 21]. Details of this model are given in ref [20]. Only the most important features are recalled here. Channel couplings in the continuum and correlation between the ejected electron and the remaining ones are neglected. Only K electrons are supposed to be ionized or promoted, so that interferences between direct and conjugate terms can be ignored due to propensity rules. Energy differential cross sections defined for a photon energy ω, with respect to the photoelectron energy ϵ, are then written as the incoherent sum of direct and conjugate partial contributions:

$$\sigma(\epsilon;\omega) \approx \sum_f (\sigma_f^D(\epsilon;\omega) + \sigma_f^C(\epsilon;\omega)) \tag{1}$$

They are modeled in the length gauge. They are given, in atomic units, by the following equations:

$$\sigma_f^D(\epsilon;\omega) = \frac{g}{3}\, 4\pi^2\alpha\, \frac{(BE_f+\epsilon)^2}{\omega}\, \rho_f^D(\epsilon) |S_{fK}|^2\, \delta(\omega - (BE_f+\epsilon);\Gamma_f) \tag{2}$$

$$\sigma_f^C(\epsilon;\omega) = \frac{g}{3}\,4\pi^2\alpha\,\frac{(BE_f+\epsilon)^2}{\omega}\,\rho_f^C(\epsilon)|D_{fK}|^2\,\delta(\omega-(BE_f+\epsilon);\Gamma_f) \qquad (3)$$

where the factor $\frac{1}{3}$ comes from the average over molecular orientations, and the multiplicity factor g comes from the number of carbon atoms implied in the model. The BE_f energies are the binding energies of the final states, and $\delta(\Omega;\Gamma_f)$ is the Lorentzian function taking into account the lifetime Γ_f of the double core hole states. The S_{fK} term is the overlap integral between the (N-1) electron final state and the initial state from which a K-electron has been annihilated. The D_{fK} term is the dipolar matrix element between the two same states. These (N-1) building blocks were calculated thanks to an original Post Hartree Fock Configuration Interaction (CI) home-made package. The $\rho_f^D(\epsilon)$ and $\rho_f^C(\epsilon)$ functions are respectively the direct and the conjugate densities. They are defined as:

$$\rho_f^D(\epsilon) = \rho_f(\epsilon)\sum_\mu |d_{\epsilon K}^\mu|^2 \;\; and \;\; \rho_f^C(\epsilon) = \rho_f(\epsilon)|s_{\epsilon K}|^2 \qquad (4)$$

where $\rho_f(\epsilon)$ is the density of states in the continuum, $d_{\epsilon K}^\mu$ is the μ(x,y,z) component of the monoelectronic dipolar transition moment between the initial K-orbital and the continuum ϵ-orbital, and $s_{\epsilon K}$ is the monoelectronic overlap between the same orbitals. The continuum densities were evaluated from an adaptation of the static-exchange (STEX-HF) approximation (see [20, 21] and references therein) combined to a Stieljes imaging [25, 26] technique as described in ref [27]. Both continuum densities were derived from a modelisation for the C_2H_4 molecule. This approximation is reasonable since our previous calculations on C_2H_2 and C_2H_4 molecules indicate that they are quite independent of the nature of the chemical bond on one part, and since, on the other part, the K^{-1} experimental cross sections have the same order of magnitude, around 1 Mbarns per atom carbon, for C_2H_4 [28] and C_6H_6 [29], at a photon energy of 300 eV above threshold .

4. Computational details

Optimized geometries of the ground state of the neutral C_6H_6 molecule were carried out in the D_{6h} symmetry using the GAMESS(US) [30] package at a DFT level of theory, with the Becke three-parameter hybrid exchange [31] and the Lee-Yang-Parr gradient-corrected correlation functional [32] (B3LYP). The core-hole final states were supposed to present the same geometry than that of the initial state. The same set of orthogonal molecular orbitals was used to describe both the ground state of the neutral molecule and the double core-hole states of the singly ionized molecular ions. This set is made of RHF-SCF orthogonal orbitals optimized for the K^{-2} core-ionized state. The same approach was successfully applied recently to $K^{-2}V$ processes in the C_2H_{2n} (n=1,2,3) [9], H_2O [20], N_2 [21] and CO_2 [18] molecular species. A localized picture (two core holes on the same carbon atom) of the $K^{-2}V$ configuration was adopted. Within this localized description, the D_{6h} molecular symmetry of the benzene molecule was lowered to the C_{2v} symmetry. To account for electronic relaxation of the valence orbitals in

the double core-hole ion, an optimized basis (O-631G*) set built from that proposed by Carniato et al. [33] but augmented by (3s; 3p; 3d) diffuse functions was used for the core-ionized carbon atom. A 6-311G* basis set was employed for the surrounding carbon and hydrogen atoms. The choice of a unique reference set of molecular orbitals allows a simpler identification and evaluation of the building blocks S_{fK} and D_{fK} . However, as this set is neither optimized for the initial, nor for the final molecular species, large CI expansions were necessary to compensate for this defect. Double core-hole final states were expanded over single up to triple valence-valence excitations. As for the initial state, it was expanded over single up to double valence-valence, but also over core-valence excitations. These latter are the only ones likely to generate direct contributions. Single point energies were also calculated for the $K^{-2}V$ states at ΔSCF and ΔKS (DFT/B3LYP) levels of theory. An aug-cc-pV5Z basis set [34] was then used for carbon and hydrogen atoms in order to describe properly relaxation and correlation effects. ΔSCF and ΔKS implementations rely on a unique $K^{-2}V$ configuration for each double core-hole final state, and therefore enable examination of the properties of the outermost valence molecular orbitals V. The V MOs associated to a direct contribution are of anti-bonding a_1^* symmetry. Those associated to a conjugate contribution can be of anti-bonding a_1^*, or b_1^*, or b_2^* symmetry.

5. Results and discussion

5.1. $K^{-2}V$ experimental results

The formation and decay of $K^{-2}V$ states are described by :

$$\begin{aligned} C_6H_6 + h\nu &\rightarrow C_6H_6^+(K^{-2}V) + e_{ph} \\ &\rightarrow C_6H_6^{2+}(K^{-1}v^{-2}V) + e_{Auger_1} \\ &\rightarrow C_6H_6^{3+}(v^{-4}V) + e_{Auger_2} \end{aligned} \quad (5)$$

where v designates a valence shell and V an unoccupied shell. The two core holes of the DCH $K^{-2}V$ state are expected to decay sequentially in a similar way as the K^{-2} DCHs do, but in the presence of the V spectator electron. The energies of the Auger electrons are thus predicted to be similar to what is measured at (e_{Auger_1}, e_{Auger_2}) = (∼300 eV , ∼240 eV) for the decay of K^{-2} DCHs [7, 5] and slightly faster by a few eV due to the screening by the V electron. A multi-coincidence data set was obtained at a photon energy of 710 eV, ∼63 eV above the DCH threshold at 647.7 eV. In order to isolate reaction (5) we select coincidences between three released electrons.

Fig.1 (panel a) shows the energy correlation between two of these electrons when the third one lies in the 200-260 eV energy range (which corresponds to the expected energy range of the Auger electron e_{Auger_2} released in the last step (1) . The horizontal lines around (x,y) = (300 eV, 70 eV) correspond to the (e_{Auger_1}, e_{ph}) pair and reveal the DCH $K^{-2}V$ states. The vertical strip around (x = 305 eV, y < 63 eV) corresponds to the faster Auger electron in coincidence with one of the two photoelectrons emitted

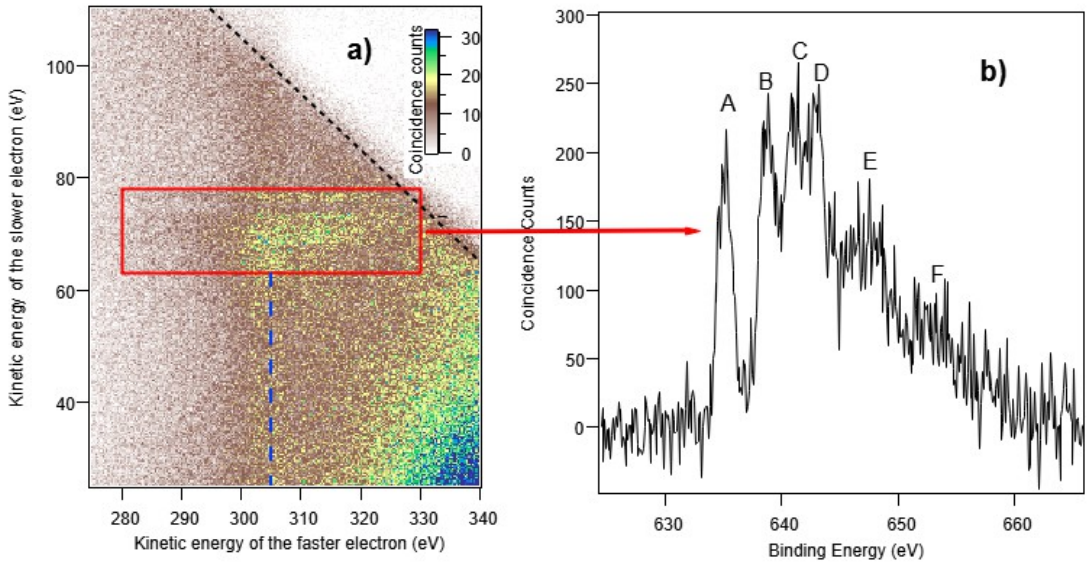

Figure 1. Panel a): Evidence for $K^{-2}V$ formation in C_6H_6: Energy correlation between two electrons detected in coincidence with a third one of (200-260 eV). The $K^{-2}V$ process appears as horizontal lines around (x,y) = (300 eV, 70 eV) inside the red rectangle. It is observed in continuity with the K^{-2} DCH formation (vertical line at x = 305 eV). The dotted diagonal line reveals the core valence double ionization path. See text for further details. A multi-coincidence dataset was accumulated for ∼12h at a photon energy of 710 eV; only 3 electron coincidences are considered here. Panel b): $K^{-2}V$ (black line) experimental photoelectron spectrum of C_6H_6 as a function of the binding energy $h\nu$-$\epsilon(e_{ph})$.

in the core double photoionization process:

$$\begin{aligned} C_6H_6 + h\nu &\rightarrow C_6H_6^{2+}(K^{-2}) + e_{ph_1} + e_{ph_2} \\ &\rightarrow C_6H_6^{3+}(K^{-1}v^{-2}) + e_{Auger_1} \\ &\rightarrow C_6H_6^{4+}(v^{-4}) + e_{Auger_2} \end{aligned} \quad (6)$$

It is observed in Fig.1 in continuity with the $K^{-2}V$ states. This describes the fact that K^{-2} DCH states can be viewed as the continuity of the $K^{-2}V$ states when one K shell electron is promoted to a higher and higher excited V orbital, up to the point it is emitted. Four electrons are emitted in reaction (2, see eq.6) but the signal appears also in the three electron coincidences events of Fig.1, when one of the photoelectrons fails to be counted due to the 70% detection efficiency. Finally one observes diagonal lines in Fig.1 such as the one represented by the dotted line. They reveal the core valence double ionization paths:

$$\begin{aligned} C_6H_6 + h\nu &\rightarrow C_6H_6^{2+}(K^{-1}v^{-1}) + e_{ph_1} + e_{ph_2} \\ &\rightarrow C_6H_6^{3+}(v^{-3}) + e_{Auger_2} \end{aligned} \quad (7)$$

The diagonal lines correspond to the photoelectron pairs $(x, y) = (e_{ph_1}, e_{ph_2})$ emitted in (3, see eq.7) One can see by comparing reactions (5) and (7) that similar $C_6H_6{}^{2+}(K^{-1}v^{-1})$ intermediate states are reached in both cases, although more excited

core valence states are expected to be reached in (5). It shows that DCH $K^{-2}V$ states can also be considered as resonances in the core valence double ionization process.

Fig.1 (panel b) shows the experimental spectrum of the $K^{-2}V$ process. This profile is obtained from Fig.1 (panel a) by the projection onto the y axis of the coincidence counts in the band x=(270-320 eV) which corresponds to kinetic energy range of the first released Auger electron e_{Auger_1} in (1). The contribution of the core valence double ionization path (3) has been subtracted; it was estimated outside of this selected band for each $C_6H_6^{2+}(K^{-1}v^{-1})$ state. The experimental spectrum exhibits four sharp bands (labeled A-to-D) with similar intensities in the low-binding energy region (630-642 eV), while the high energy region shows broader components (regions E-F).

The experimental integrated cross section for the formation of the $K^{-2}3b_1^*$ state (area under the peak A) could be derived on an absolute scale thanks to the branching ratio $K^{-2}V$(peak A)/K^{-1} on one part and to the absolute cross section for the photoionization K^{-1} process on the other part. The ratio was estimated about $12\times10^{-5}\pm20\%$ in this work at a photon energy of 710 eV. The K^{-1} cross section in C_6H_6 was assumed to be 678 kbarns, six times the K^{-1} cross section referenced by Veigele [36] for the carbon atom at 700 eV (6×113 kbarns). So that the $K^{-2}3b_1^*$ cross section could be estimated about 81 ± 16 barns.

5.2. $K^{-2}V$ theoretical results

.

5.2.1. Binding Energies Theoretical ΔSCF, ΔKS and CI-SDT binding energies of the lowest lying $K^{-2}V$ states are collected in Table I, and compared with experimental results from Fig.1 (b). Relativistic effects (0.1 eV/hole [13]) were taken into account in all the modelisations. Term values (TV), which are the distances from the K^{-2} threshold, are given in parentheses. CI-SDT results come from our home made package. The binding energies of the lowest energy state of each A_1, B_1, and B_2 symmetry were determined thanks to a large CI-SDT implementation taking into account 115 virtual MOs and were used as the reference values for each series. Inside each of the three series the binding energies of the higher energy states were obtained from their relative energy distance with the lowest energy state, evaluated thanks to CI-SDT implementations taking into account 115 virtuals for single (S) and double (D) excitations and only 20 virtual orbitals for triple (T) excitations, added to the reference value of the corresponding series.

ΔSCF and ΔKS results come from GAMESS(US) [30] outputs. The ΔKS binding energies are underestimated relatively to experimental values by about 2 eV. This difficulty for density functional computations to reproduce well double core-hole experimental values has been already observed [13, 17]. The ΔKS Term Values are however in good agreement with experimental ones. Conclusions concerning the comparisons of experimental results with ΔSCF binding energies and TV are reversed.

Table 1. Theoretical ΔSCF, ΔKS with a large aug-cc-pV5Z basis set and CI-SDT with a 6-31G* basis set binding energies of the lowest lying $K^{-2}V$ states of A_1, B_1, and B_2 symmetry are given in eV. Term values (TV) are given in parentheses in eV. CI-SDT modelisations were performed with a large active space including 15 doubly occupied and 115 virtual orbitals for the lowest energy state of each symmetry. The corresponding values are labeled in **bold** characters. The binding energies inside each series were obtained thanks to CI-SDT modelisations with a smaller active space including 115 virtuals for single (S) and double (D) excitations and only 20 virtual orbitals for triple excitations (T) (see text for details). [a] For calculation of binding energies a O-631G* basis set as optimized by Carniato et al [33] augmented by (3s,3p,3d) diffuse orbitals is used for the double core hole carbon. The standard 6-31G* basis set as optimized by Pople et al.[35] for the neutral state of carbon augmented by (3s,3p,3d) diffuse orbitals for size consistency between initial and final states was used for the ground state description.

State	Label	ΔSCF	ΔKS	CI-SDT	Exp
		Aug-cc-pV5Z		631G*[a]	
Region A					
$1B_1$	(a)	634.75 (11.35)	632.81 (12.17)	**635.26 (11.57)**	634.50±1 (13.2±1)
Region B					
$1A_1$	(b)	638.07 (8.03)	636.23 (8.75)	**638.83 (8.00)**	638.15±1 (9.55±1)
Region C					640.40±1 (7.30±1)
$2A_1$	(c)	640.28 (5.82)	638.32 (6.66)	640.92 (5.91)	
$2B1$	(d)	640.65 (5.45)	639.05 (5.99)	641.08 (5.75)	
$1B_2$		640.63 (5.47)	638.71 (6.27)	**641.16 (5.67)**	
$3A_1$	(e)	641.05 (5.05)	638.56 (6.42)	641.33 (5.50)	
$2B_2$	(f)	641.45 (4.65)	639.10 (5.88)	641.67 (5.16)	
$4A_1$		641.29 (4.81)	639.02 (5.96)	641.84 (4.99)	
Region D					642.20±1 (5.50±1)
$3B1$		642.17 (3.93)	640.06 (4.92)	642.44 (4.39)	
$3B_2$	(g)	642.39 (3.71)	640.63 (4.35)	642.61 (4.22)	
$5A_1$	(h)	642.21(3.89)	639.90 (5.08)	642.91 (3.92)	
$6A_1$	(i)	642.64 (3.46)	640.35 (4.63)	643.39 (3.44)	
K^{-2}		645.90	644.98	646.83	647.70±1

Even if the ΔSCF procedure does not take into account electronic correlation effects, the ΔSCF binding energies are closer to experimental values than the ΔKS ones. This unexpected agreement probably comes from a compensation of valence-valence correlation effects in the final state by core-core and core-valence correlation effects in the initial state. CI-SDT modelisations provide binding energies and TV in overall good agreement with experimental values.

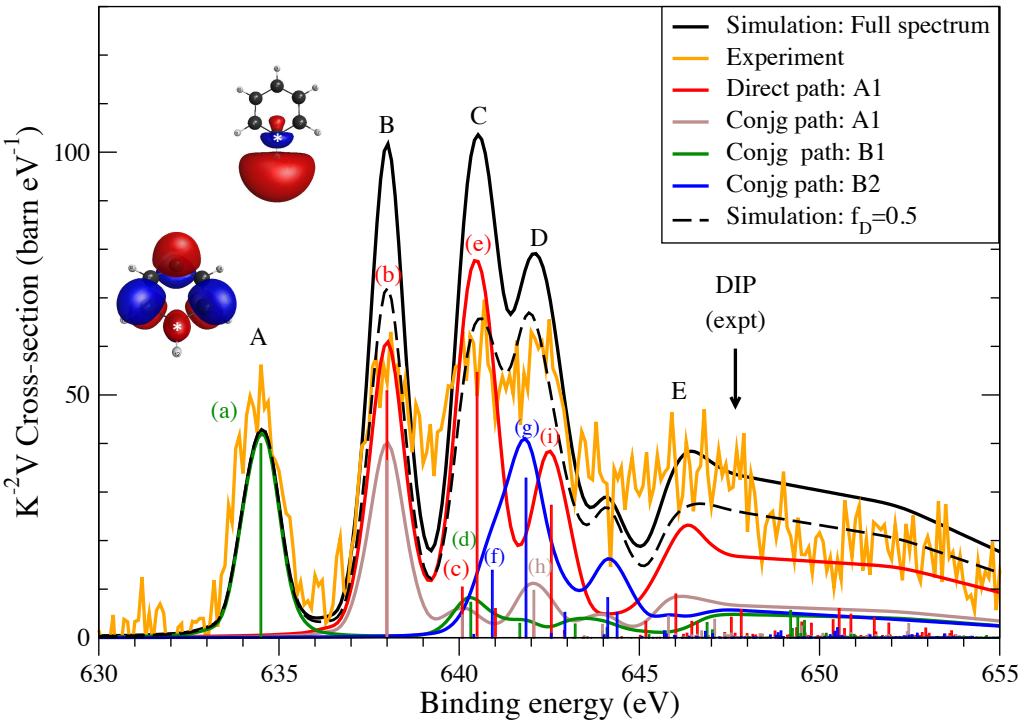

Figure 2. Comparison of experimental and theoretical $K^{-2}V$ spectra. The theoretical spectrum is modeled thanks to the CI-SDT scheme, taking into account a lifetime γ=0.27 eV and an experimental resolution of 1.3 eV FWHM. The red line represents the direct contribution (A_1 symmetry), the green, brown and blue lines represent the conjugate contributions of respectively B_1, A_1, and B_2 symmetry. The black line represents the incoherent sum of direct and conjugate contributions. Electronic density plots are displayed for the two first peaks (a) and (b). Dashed line: full theoretical spectrum where mono-electronic dipole moments associated to the Direct path are divided by a factor (f_D=0.5) two from their calculated absolute initial values

5.2.2. Photoelectron spectrum The $K^{-2}V$ theoretical profile giving absolute cross-sections is displayed in Fig.2. The formal theoretical cross sections were obtained from equations (2) and (3) with a lifetime Γ=0.27 eV. This value is approximatively three times the lifetime of the 1s core hole in the carbon atom (this factor of three is discussed in ref [22]). These cross sections were then convoluted by a gaussian factor of 1.3 eV FWHM to simulate the experimental resolution. On Fig.2 the whole CI spectrum was shifted by scaling the theoretical position of the peak A to the experimental energy (634.5 eV). The DIP (double ionization potential) is settled at the experimental value of 647.7 eV. The letters from A to E reproduce the labels used in Fig.1 to identify the main experimental structures. The bars indicate the energy

position of the principal $K^{-2}V$ states labeled from (a) to (i). The green and blue colors apply to pure conjugate components of respectively B_1 and B_2 symmetry. The red color applies to components of A_1 symmetry. They can have either a pure direct ((e) and (i)), or a pure conjugate (h) origin, or even be reached by both the direct and conjugate paths ((b) and (c)). The absolute scale is fixed by the theoretical cross sections. The intensity of the experimental spectrum has been scaled so that the cross section for the excitation of the LUMO (area under the peak (a)) corresponds to the value of 81 barns, while the theoretical cross section was obtained about 65 barns. The theoretical profile reproduces with a good agreement the position of the four main structures A to D observed experimentally below the DIP, as well as the broad structure E around this threshold. The overall agreement of the absolute scales is good. There is some discrepancy concerning the relative intensities of the peaks A and B and of the peaks C and D. These relative intensities are very dependent on the relative strength of direct and conjugate components ([42]), and more particularly of the continuum densities appearing in eq.4. In fig.2 we have reported (dashed line) the full theoretical spectrum where mono-electronic dipole moments associated to the Direct path were divided by a factor two from their absolute initial values (f_D=0.5). As observed, a better agreement between theory and experiment is reached for regions B/C/D in which direct transitions play a major role.

Anyway, we have confidence in this absolute scale because, first, experimental and theoretical determinations are in very good agreement, and second, this scale corresponds to a value about 25 barns per double bond, which coincides with a previous value we determined for the $K^{-2}V$(LUMO) in the C_2H_4 molecule [17].

Each of the two first structures A and B is made of a unique peak respectively (a) and (b). The first peak (a) corresponds to a conjugate component where an excitation towards the $3b_1^*$ LUMO is involved mainly. Such a similar excitation takes place in the C1s NEXAFS spectrum [29, 37, 38, 39] of C_6H_6. The peak (b) corresponds principally to an excitation towards the first unoccupied MO of symmetry a_1^*, ($13\ a_1^*$) that can be reached by both the direct and the conjugate channels. Direct (red line) and conjugate (brown line) contributions add up to lead to a profile B of symmetry A_1 more intense than the neighboring profile A of symmetry B_1. This is quite singular as $1s\rightarrow \sigma^*$ lines are usually weak compared to $1s\rightarrow \pi^*$ ones in standard Carbon K-edge NEXAFS spectra [37].

Electronic density plots are displayed on Fig.2 for the $3b_1^*$ and $13a_1^*$ anti-bonding MOs. The electronic density of the LUMO ($3b_1^*$) is localized out of the plane of the benzene ring. Some amount of electronic density can be observed on the double core-hole carbon atom marked with an asterisk. This migration is however weak. An analysis of Löwdin populations for the LUMO orbital indicates an electronic density of only 11% on the double core-hole atom in the $K^{-2}V$ case, half of the density observed in the $K^{-1}V$ case. This comparison reveals, as expected, a more pronounced anti-bonding character of the LUMO in the $K^{-2}V$ species than in the $K^{-1}V$ one. The most important part of the electronic density transfer towards the double core-hole carbon atom (+1.81 electrons)

is operated from the doubly occupied deeper valence MOs. The electronic density plot of the first MO of symmetry a_1^* (13 a_1^*) shows that a significant part of the electron density is localized along the C-H bond of the double core-hole carbon, according to an anti-bonding scheme. An analysis of Löwdin populations indicates an electronic density of 34% around the double core-hole carbon with large s/p/d hybridization (13% for s, 13% for p and 8% for d_z^2 respectively) and 33% around the hydrogen atom. The electronic transfer from the deep doubly occupied deeper valence MOs is reduced to 1.66 electrons.

The two MOs $3b_1^*$ and $13a_1^*$ correspond to compact orbitals of dominant valence character. This property is supported by the small values of mean-squared radius $< r^2 >$, ≈2.3 Åand ≈2.26 Åfor respectively $3b_1^*$ and $13a_1^*$ MOs.

The structure C is mainly composed of three components with different symmetries. The main conjugate line of symmetry B_1 ($2B_1$) is around 640.32 eV (d), the main direct line ($3A_1$) is around 640.57 eV (e), the main conjugate line of symmetry B_2 ($2B_2$) is around 640.91 eV (f). The majority of these lines correspond to the mixing of at least two main configurations. The mean-squared radius $< r^2 >$ of the corresponding MOs are large (≈4.5 Å), indicating a diffuse Rydberg character.

The structure D is mainly composed of two components, a conjugate line (of symmetry B_2 ($3B_2^*$) at 641.85 eV (g), and a direct line ($6A_1$) at 642.63 eV (i).

The structure E is close to the double inner-shell ionization threshold (DIP) presents a collection of K^{-2}V-V'$^{-1}$V" satellite lines where a supplementary V'→V" excitation takes place. For example the $K^{-2}3b_1^*7b_2^{-1}2a_2$ configuration has been identified, where the $2a_2$ MO of large diffuse character is populated.

6. AUGER DECAY OF $K^{-2}V$ STATES

As can be seen in Fig.1 (710eV), it is possible to select a given $K^{-2}V$ state (peaks A to C) and to obtain its high kinetic energy Auger decay spectrum by projecting the corresponding horizontal line in the 2D map onto the X-axis. It is even easier to select, among all three-electron coincidence events, the photoelectron in the energy range of a given state to obtain directly the total Auger spectra corresponding to the 2-steps Auger decay. However, with a relative energy resolution ΔE/E of 1.6% the energy resolution around 300 eV is limited to about ∼5eV and gives only a broad structure as observed in fig. 1 in ref. [13]. To improve the absolute energy resolution of the Auger electrons, we decelerate the electrons in the MB-TOF with -200V potential applied to the 2m long fight tube.

A direct illustration of the power of the deceleration method is shown in Fig.3 (b) with the Auger spectrum of benzene at hν=590 eV. This spectrum is deduced from the coincidence between the K^{-1} photoelectron and the Auger electron. This spectrum is totally comparable to the original spectrum [41] that was interpreted by Tarantelli *et al.* [40] and latter measured by Rennie *et al.* [29] (Fig.3 (d)), the energy resolution and a 50meV integration step are good enough to observe all the structures. Due to

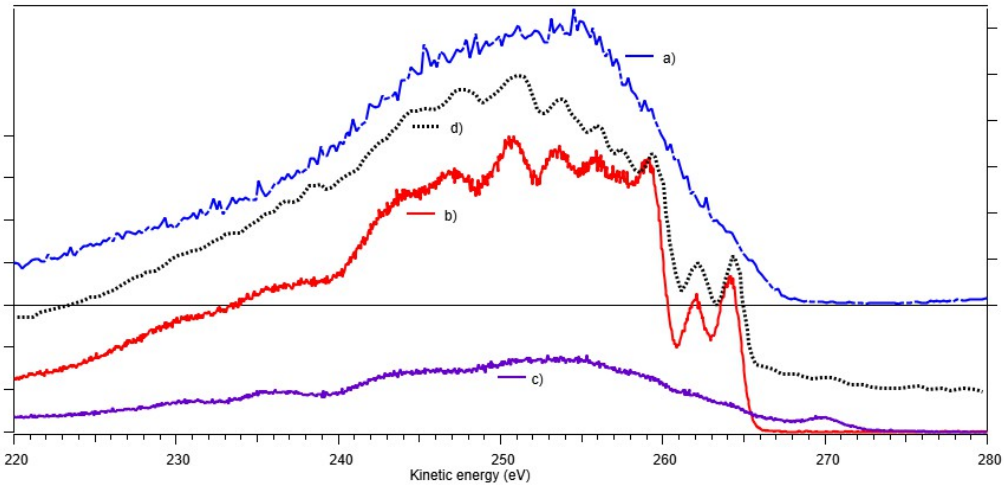

Figure 3. Auger spectra of benzene deduced from coincidence between the C(1s) photoelectron and the Auger electron at 510 eV photon energy. Without deceleration the resolution is about 4 eV (blue line a). With 200eV deceleration the resolution is about 1eV (red line b) and the Auger spectrum exhibits the same structures with comparable resolution than the one found in literature [29] at 390eV photon energy (black dotted line d). The specific Auger spectrum from satellite states is also shown (violet line c) and we can see the participator Auger in the 267 eV shoulder.

the detection in coincidence of the Auger electron with the K^{-1} photoelectron, the contribution to the Auger spectra of the decay from satellite states is cleared up and the shoulder above 267eV and the background disappear in Fig.3 (b). To go further, it was also possible to extract, for the first time, the Auger decay of $K^{-1}v^{-1}V$ satellite states lying from 3 to 11 eV above the the K^{-1} ionization threshold [29] as seen in Fig.3 (c).

Concerning the Auger decay of $K^{-2}V$ states , the energy resolution for 300 eV Auger electrons decelerated to about 100 eV should be 1.6 eV. Since, to extract the $K^{-2}V$ process from the whole dataset it is still necessary to detect the three electrons emitted in (eq 18), the photoelectron must have more than 200 eV kinetic energy (KE) and the photon energy must also be adjusted to shift the photoelectron energy out of the energy range of the two Auger electrons. At a photon energy of 855 eV, the C(1s) photoelectron has less than 220 eV KE and is also slower than the slowest Auger electron.

At 855 eV photon energy, with 200V retardation of all the electrons, the energy resolution is sufficient to isolate the $K^{-2}V$ states, as well as at hν=710eV without retardation. By selecting the photoelectron corresponding to the three better resolved A, B and C structures, we can extract the specific Auger decay of each state with a good resolution. We obtain the fast and slow Auger electron spectra shown in Fig. 4. To make the comparison easier, we also plot the normal K^{-1} Auger spectrum.

Considering the very weak process we are looking at, the statistics is rather good, the two Auger decay steps of selected states can be clearly identified and differences are visible for the different $K^{-2}V$ peaks A, B and C. Compared to the hypersatellite

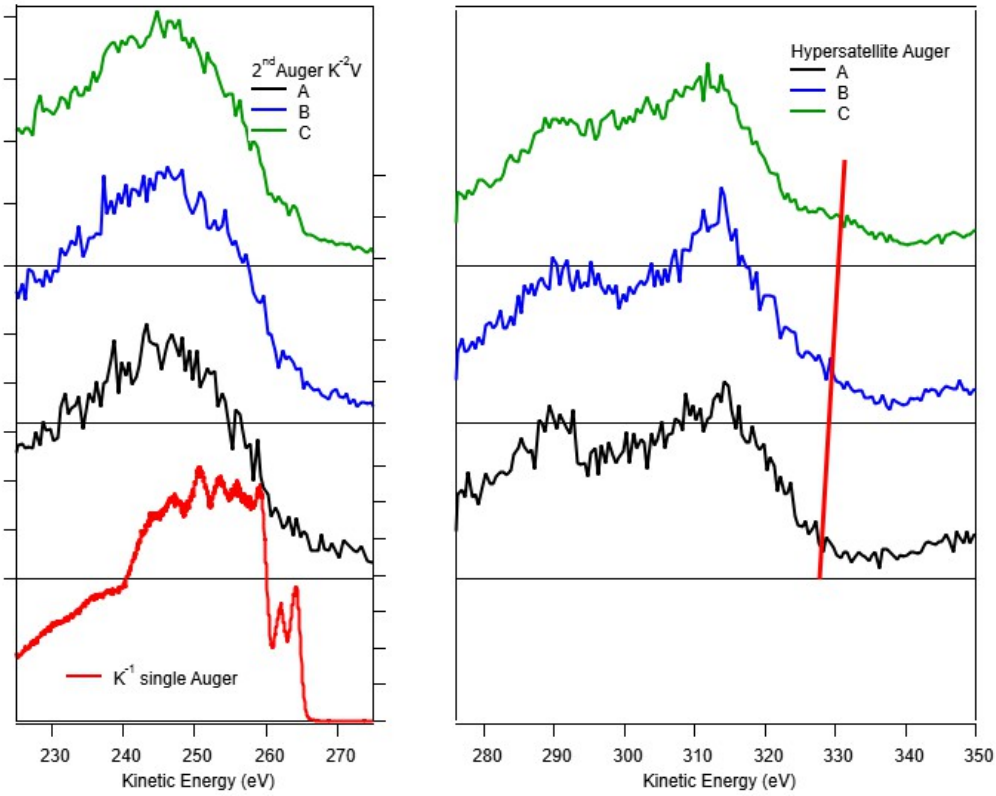

Figure 4. Auger spectra following $K^{-2}V$ ionization/excitation process on peaks A, B and C. The integration step was 500 meV. The K^{-1} normal Auger spectrum (red line) is also obtained with an integration step of 50meV and a good resolution (1 eV) and serves as a calibration reference for the Auger spectra due to $K^{-2}V$.

Auger spectra of K^{-2} states (Fig. 1 in ref. [1]) the better resolution allows to identify two peaks in the hypersatellite Auger spectra. The hypersatellite Auger spectra in the $K^{-2}V$ case is shifted by about 10eV with respect to the K^{-2} hypersatellite Auger peaks [22] due to the screening of the outer V electron. What is also visible on the high energy wing is a shoulder that shifts (red line) with the state considered. That corresponds most probably to the participator Auger decay of the V electron in the first Auger decay.

The Auger electron emitted in the second step of the cascade is slower with an energy close to the normal K^{-1} Auger electron. No clear structure can be observed although the resolution is very good as can be seen for the normal K^{-1} Auger spectrum. As was observed for K^{-2} in C_2H_2 [5] it is also possible that dissociation or elongation of the carbon ring occur after the first Auger decay and broaden the distribution of the second Auger electron. At the present stage of the theory, it was not possible to calculate the specific Auger spectra of $K^{-2}V$ states but the quality of our results, that is possible due to three-electron coincidence with high resolution due to retardation of all three electrons, could certainly stimulate theoreticians.

7. Summary

In summary, we have reported here the experimental and theoretical analysis of $K^{-2}V$ satellite spectra in the C_6H_6 molecular system. We have also been able to observe the specific two-step Auger decays of $K^{-2}V$ selected states with good resolution.

The recorded $K^{-2}V$ spectrum converging toward the double-core K^{-2} ionization threshold is composed by four main resonances, revealing clear signatures of direct (monopolar) and conjugate (dipolar NEXAFS-like) shakeup lines of comparable magnitude as already observed in acetylene, ethylene and ethane [17] or in N_2 [21].

The first resonance is unambiguously assigned to the π-type (b_1^*) antibonding valence state while the three others resonances are mainly made up of σ-type (a_1-a_1^*) states with out-of-plane b_1 and in-plane b_2 conjugate lines. It would also be interesting to compare the present experimental and theoretical study to possible experiments involving two-photon processes on XFELs sources. In a two-photon one-color ionization + excitation scheme, it is possible to scan the photon energy to explore the excitation of $K^{-2}V$ resonances from the K^{-1} ionized ion created by absorption of a first photon. One could observe cancellation of the direct shakeup channels (red solid lines).

8. Aknowledgments

The experiments presented here were performed at SOLEIL at the SEXTANTS beamline with the approval of the Soleil Peer Review Committee (Project Nos. 20140129 and 20171368). We are grateful to the SEXTANTS scientists for help during the measurements and to SOLEIL staff for stable operation of the storage ring during the experiments. K.I. acknowledges the support of the Labex PLAS@PAR, managed by the Agence Nationale de la Recherche, as part of the Programme d′Investissements d′Avenir under Reference N. ANR-11-IDEX-0004-02. N.B. acknowledges the support of the Chemical Sciences, Geosciences, and Biosciences Division, Office of Basic Energy Sciences, Office of Science, U.S. Department of Energy, Grant No. DE-SC0012376.

9. References.

[1] L. Young, E. P. Kanter and B. Krässig, Nature (London) **466**, 56 (2010)
[2] J. H. D. Eland, M. Tashiro, P. Linusson, M. Ehara, K. Ueda and R. Feifel, Phys. Rev. Lett. **105** 213005 (2010)
[3] L. Fang *et al.*, Phys. Rev. Lett. **105**, 83005 (2010)
[4] P. Lablanquie *et al.*, Phys. Rev. Lett. **106**, 063003 (2011)
[5] M. Tashiro, M. Nakano, M. Ehara, F. Penent, L. Andric, J. Palaudoux, K. Ito, Y. Hikosaka, N. Kouchi and P. Lablanquie, J. Chem. Phys. **137**, 224306 (2012)
[6] N. Berrah et al., Proc. Natl. Acad. Sci. U.S.A. **108**, 16912 (2011)
[7] P. Lablanquie *et al.*, Phys. Rev. Lett. **107**, 193004 (2011)
[8] P. Salen *et al.*, Phys. Rev. Lett. **108**, 153003 (2012)
[9] M. Nakano *et al.*, Phys. Rev. Lett. **110**, 163001 (2013)
[10] L. Hedin, M. Tashiro, P. Linusson, J.H.D. Eland, M. Ehara, K. Ueda, V. Zhaunerchyk, L.Karlsson, K. Pernestal and R. Feifel, J. Chem. Phys. **140**, 044309 (2014)

[11] L. S. Cederbaum, F. Tarantelli, A. Sgamellotti and J. Schirmer, J. Chem. Phys. **85**, 6513 (1986)
[12] R. Santra, N. V. Kryzhevoi and L. S. Cederbaum, Phys. Rev. Lett. **103**, 013002 (2009)
[13] S. Carniato *et al.* J. Chem. Phys. **151**, 214303 (2019)
[14] L. S. Cederbaum, F. Tarantelli, A. Sgamellotti and J. Schirmer, J. Chem. Phys. **86**, 2168 (1987)
[15] M. Tashiro, M. Ehara, H. Fukuzawa, K. Ueda, C. Buth, N. V. Kryzhevoi,L. S. Cederbaum, J. Chem. Phys. **132**, 184302 (2010).
[16] A. Ferté *et al.*, J. Phys. Chem. Lett. **11**, 4359 (2020)
[17] M. Nakano, P. Selles, P. Lablanquie, Y. Hikosaka, F. Penent, E. Shigemasa, K. Ito and S. Carniato Phys. Rev. Lett. **111**, 123001 (2013)
[18] Carniato *et al.*, Phys Rev A **94**, 013416 (2016)
[19] B. Kempgens, A. Kivimäki, M. Neeb, H. M. Köppe, A. M. Bradshaw and J. Feldhaus, J. Phys. B **29**, 5389 (1996)
[20] S. Carniato *et al.*, J. Chem. Phys **142**, 014307 (2015)
[21] S. Carniato*et al.*, J. Chem. Phys. **142**, 014308 (2015)
[22] G. Goldsztejn *et al.*, Phys. Rev. Lett. **117**, 133001 (2016)
[23] R. Feifel *et al.*, Scientific Reports **7**, 13317 (2017)
[24] S. G. Chiuzbăian *et al.*, Rev. Sci. Instrum. **85**, 043108 (2014).
[25] P. W. Langhoff, B. J. Dalton, S. M. Grimes, J. P. Vary and S. A. Williams, editors, *Theory and Application of Moment Methods in Many-Fermions Systems*, page 191. Plenum, New-York,1980.
[26] I. Cacelli *et al.*, *In Modern Techniques in Computational Chemistry*: MOTECC-91, page 695. E. Clementi, editor, Escom, Leiden, 1991 and references therein.
[27] H. Ågren, V. Caravetta and L.G.M Pettersson, Theor. Chem. Acc **97**, 14 (1997)
[28] B. Kempgens, H. M. Köppe, A. Kivimäki, M. Neeb, K. Maier, U. Hergenhahn, and A. M. Bradshaw, Phys. Rev. Lett. **79**, 35 (1997).
[29] E. E. Rennie *et al.*, J. Chem. Phys. **113** 7362 (2000).
[30] M. W. Schmidt *et al.*, J. Comput. Chem. **14**, 1347 (1993)
[31] A. D. Becke, J. Chem. Phys. **98**, 5648 (1993)
[32] C. Lee, W. Yang and R. G. Parr, Phys. Rev. B, **37**, 785 (1988)
[33] S. Carniato and P. Millie, J. Chem. Phys. **116**, 3521 (2002)
[34] D. E. Woon and T. H. Dunning Jr., J. Chem. Phys. **103**, 4572 (1995)
[35] W. J. Hehre, R. Ditchfield, and J. A. Pople, J. Chem. Phys. **56**, 2257 (1972??)
[36] Wm. J. Veigele, At. Data and Nucl. Data Tables **5**, 51 (1973)
[37] J.P Doering , A. Gedanken, A. P. Hitchcock, P. Fischer, J. Moore, J.K. Olthoff, J. Tossel, K. Raghavachari and M. B. Robin, J. Am. Chem. Soc. **108**, 3602 (1986)
[38] R. Püttner, C. Kolczewski, M. Martins, A.S. Schlachter, G. Snell, M. SantAnna, J. Viefhaus, K. Hermann, G. Kaindl, Chem. Phys. Lett. **393**, 361 (2004).
[39] B. Kempgens, B.S. Itchkawitz, J. Feldhaus, A.M. Bradshaw, H. Köppel, M. Döscher, F.X. Gadea, L.S. Cederbaum, Chem. Phys. Lett. **277**, 436 (1997)
[40] F. Tarantelli, A. Sgamellotti and J. Schirmer, J. Chem. Phys. **86**, 2201 (1987)
[41] K. Siegbahn *et al. ESCA applied to free molecules*, North Holland, Amsterdam, (1969).
[42] S. Carniato, J. Electron Spectrosc. Relat. Phenom. **239** 146931 (2020)